ACS Photonics

Letter

pubs.acs.org/journal/apchd5

Nonlinear Symmetry Breaking in Symmetric Oligomers

Mohsen Rahmani,*[,†] Alexander S. Shorokhov,[‡] Ben Hopkins,[†] Andrey E. Miroshnichenko,[†] Maxim R. Shcherbakov,[‡] Rocio Camacho-Morales,[†] Andrey A. Fedyanin,[‡] Dragomir N. Neshev,[†] and Yuri S. Kivshar[†]

[†]Nonlinear Physics Centre and Centre for Ultrahigh Bandwidth Devices for Optical Systems (CUDOS), Research School of Physics and Engineering, The Australian National University, Canberra, ACT 2601, Australia

[‡]Faculty of Physics, Lomonosov Moscow State University, 119991 Moscow, Russia

Supporting Information

ABSTRACT: A novel type of nonlinear symmetry breaking in symmetric plasmonic oligomers is reported. By monitoring the strength of the second-harmonic signal while changing the polarization angle of the pump, we observe nonlinear symmetry breaking as a large variation in the generated nonlinear signal. Importantly, the strongly anisotropic nonlinear response is produced by a symmetric structure with isotropic linear response when rotating polarization. We provide theoretical analysis to describe and characterize this effect. Our finding opens new avenues to reveal and characterize the symmetry of nanoscale structures and molecules and also to remotely monitor variations of near-field patterns produced by symmetric nanostructures.

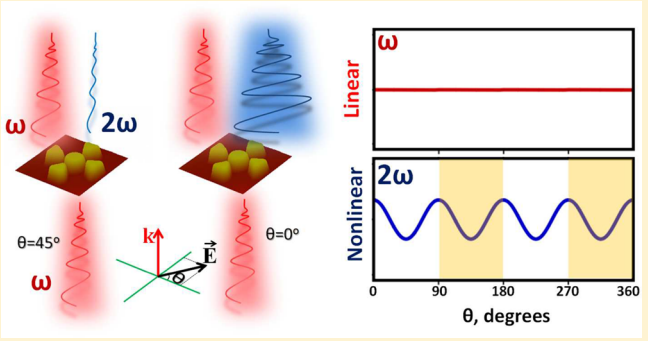

KEYWORDS: *subwavelength nanostructures, nonlinear spectroscopy, symmetry breaking, polarization-selective device*

The effect of linear symmetry breaking in nanostructures[1−4] has recently attracted much attention, especially for the studies of asymmetric metallic and dielectric nanostructures as building blocks for metamaterials and metasurfaces to realize passive[5] and active[6] photonic devices. Structural symmetry breaking can refer to an alteration of nanostructure geometry to make the system asymmetric either in-plane[7,8] or out-of-plane.[9] Altering the excitation conditions, such as changing the incident light polarization or excitation angle,[10,11] one can also produce a similar symmetry breaking effect on the fields, rather than geometry. Benefits of such asymmetry, particularly in metallic structures, such as dolmen-type arrangements of bars[12] and nonconcentric ring-disk cavities,[7] have been justified for a large number of applications ranging from ultrasensitive chemical and biological sensors[2,13] to signal processing and slow-light devices.[1]

Symmetry breaking can also occur in nonlinear regimes. One such scenario is known to occur via coupling between two modes, where optical nonlinearity shifts the resonance frequencies of the modes differently, giving birth to a new asymmetric mode. An example is the nonlinear modes of planar waveguides, which have been studied and classified in different settings, where a novel asymmetric nonlinear mode emerges via Kerr-type nonlinear symmetry breaking through bifurcation.[14] Similar symmetry breaking effects have been observed in nonlinear couplers,[15] where light can be localized in one of the arms provided the input power exceeds a critical value. Along with the study of planar structures, the nonlinearity-induced localization of plasmon beams was discussed in more complicated settings.[16−19] A common feature of these nonlinear systems is that the symmetry breaking *can affect both linear and nonlinear responses simultaneously*. Conversely, nonlinear alterations in symmetrically coupled nanoclusters with invariant linear responses have not been reported so far, to the best of our knowledge.

Aggregated nanoparticle clusters, the so-called nanoparticle oligomers, are well-known symmetric nanostructures,[20−28] with 3-fold or higher discrete rotational symmetry (C_n for $n \geq 3$), that exhibit entirely polarization-independent far-field optical properties.[28] Nanoparticle oligomers with such symmetries are of intense current interest and provide analogies for molecular physics of many organic and inorganic symmetric molecules, such as carbon in graphene networks, methane (CH_4), benzene (C_6H_6), BCl_3, and XeF_4.[21,29,30] Linear optical properties of plasmonic oligomers can provide a qualitative basis to explore the energy levels of molecular orbitals or molecule formation due to an overlap and interaction of electronic orbitals of individual atoms.[21] Nonlinear light generation from metallic and dielectric nanoparticle oligomers, at certain incident polarizations, has also recently been studied in a number of publications.[31−38] However, asymmetric nonlinear generation associated with symmetric linear responses in oligomers remains unexplored to date. In this Letter, we demonstrate

Received: November 16, 2016
Published: February 13, 2017

DOI: 10.1021/acsphotonics.6b00902
ACS Photonics 2017, 4, 454−461

that C_4 symmetry oligomers can exhibit symmetric linear and asymmetric nonlinear optical properties in the far field, simultaneously. We show that, by rotating the linear incident polarization, strongly asymmetric second-harmonic generation (SHG) takes place. Such variation is in direct correlation with the symmetry class of the oligomers, which cannot be observed in the linear far-field spectra.

One of the promising applications of our finding is employing this technique to examine more subtle structures and symmetries of nanostructures or even molecules, compared to what has previously been possible with optical far-field measurements. Indeed, it has also recently been discussed in a different approach that a nonlinear signal can be imprinted with dynamical symmetries when illuminating molecular structures through circular polarizations.[39−41] A separate application of our finding is to monitor experimentally near-field patterns of ultrasmall nanostructures, given the signature of varied near-field distributions is otherwise not reflected in linear far-field spectra due to rotational symmetry of oligomers.[28]

In this work, we focus on symmetric plasmonic pentamers with C_4 symmetry. Figure 1a demonstrates the AFM image of Au monomer and two types of pentamer arrays. Pentamer I consists of five circular disks, and pentamer II contains a central circular disk surrounded by four triangle-shaped nanoparticles. Pentamer II has been designed and fabricated to better study the effects of higher near-field enhancement in the same geometrical pentamer. For details of the fabrication procedure see the Methods section. The external diameters of all elements and interparticle gaps are ∼140 nm and ∼20 nm, respectively. The numerically simulated and experimentally measured optical responses of all configurations for polarizations of $\theta = 0°$ and $\theta = 45°$ with respect to the x-axis are displayed in Figure 1b, where θ is the polarization angle in the xy plane, as illustrated in Figure 1b. For simulation details see the Methods section. Both numerical and experimental results show clearly that the far-field optical properties are *independent of polarization*. This invariance of the extinction cross sections with polarization can be explained by the geometrical symmetry of the pentamer nanoclusters, where the effect of polarization is inherently connected to the symmetry of a scattering system.[28]

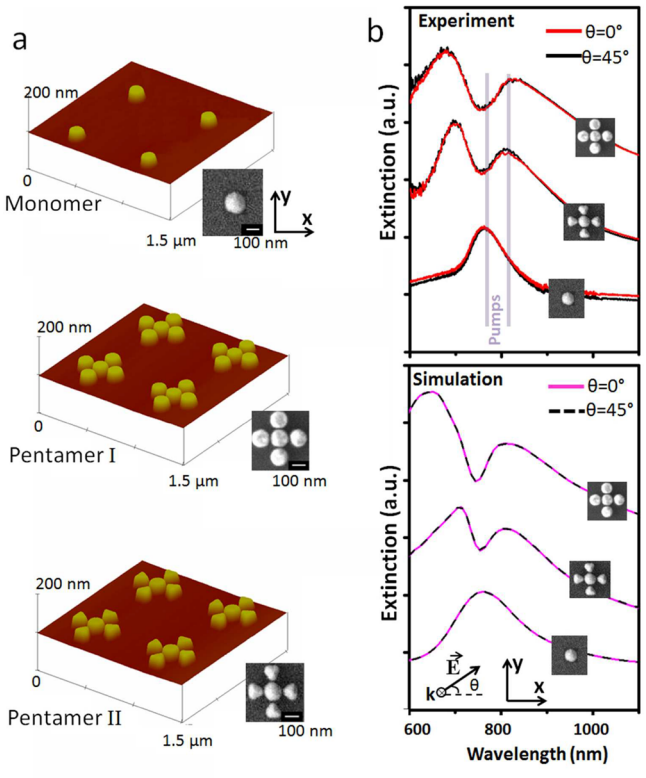

Figure 1. Demonstration of polarization-independent linear optical properties. (a) AFM images of a periodic array of fabricated monomers and pentamers (types I and II). The right insets are close-up SEM images of one unit cell. (b) Experimental extinction (1 − transmission) and numerically simulated extinction cross section spectra at the polarization directions of 0° and 45°, with respect to the x-axis. Wavelengths indicated on the experimental images show the fundamental wavelengths employed for SHG. Scale bar of SEM images is 100 nm.

The nature of different extinction peaks and dip of the optical resonance of oligomers has been studied earlier;[20−26] for example, the dip at 780 nm in our case corresponds to the Fano resonance in the linear regime.[20−26] Fano resonances in plasmonic nanostructures are produced by the interaction between linear nonorthogonal modes of the system to result in super-radiant and subradiant collective modes. A super-radiant mode can be excited directly under illumination. But a sub-radiant mode cannot interact directly with illumination; however it can be excited by the near field associated with the super-radiant mode. On the basis of a phase difference between modes, the final mode can be either attenuated or reinforced, featuring the Fano resonance.[20−26] Although a number of research papers studied the effect of the Fano resonance on the enhancement of both SHG[31] and THG[37] at certain pump polarizations, a comprehensive study on non-linear generation from various resonances and polarization excitations is still missing. To fill this gap, here we study SHG by pumping not only at the Fano resonance wavelength (780 nm) but also at the wavelength corresponding to the second peak (820 nm), where pentamers experience the highest amount of near-field enhancements in the gap.[42] In plasmonic oligomers, the second peak of the extinction curve (at the larger wavelength) is where the destructive interference between sub- and super-radiant modes vanishes. This is why near fields tend to be localized in the gaps along the polarization axis, similar to the case of a simple dimer.[21,24] For comparison, here we also consider the case of single monomers.

This trend is corroborated by the experimental nonlinear measurements. Figure 2a shows that the SHG intensity from our nonlinear system is sensitive to the second power of the fundamental incident light. As can be seen, increasing the fundamental incident power leads to an improvement in the conversion efficiency, which is a direct consequence of the scattering nature of the harmonic generation mechanisms.[43,44] However, it should be noted that this happens only for relatively low powers, and the nonlinear upconversion efficiency is closely related to the laser damage threshold of the nanosystems.[45]

Figure 2b shows the SHG signal generated from a single Au monomer pumped at its plasmonic resonance (780 nm) with rotating polarization. It is known that SHG from centrosymmetric materials is due to the breaking of inversion symmetry at their surfaces.[46] Centrosymmetry from the cubic lattice of typical plasmonic metals forbids quadratic nonlinearity in their bulk, and instead it appears only at interfaces where centrosymmetry is broken locally. Pumping at the plasmonic resonance has been justified as a versatile strategy to enhance SHG among plasmonic structures.[47,48] As expected, rotating

DOI: 10.1021/acsphotonics.6b00902
ACS Photonics 2017, 4, 454−461

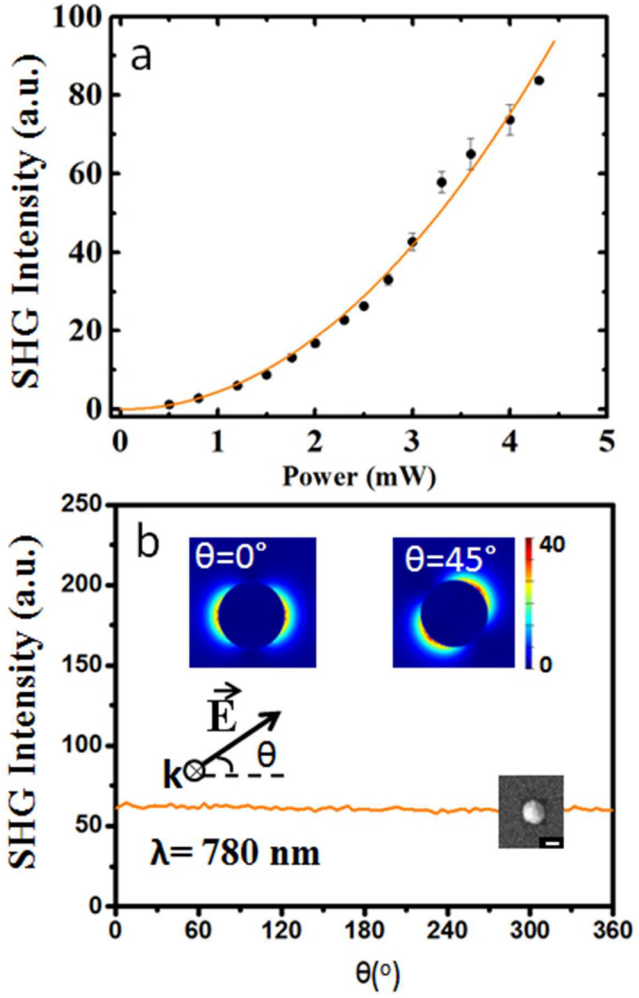

Figure 2. Second-harmonic properties from an isolated nanoparticle. (a) Evolution of second-harmonic intensity as a function of the fundamental incident power. Black dots indicate experimental data. Orange line is a numerical fit with the second-order power function, where $y = ax^p$ and $p = 2.04 \pm 0.09$. (b) Measured second-harmonic generation intensity of a monomer nanoparticle for an incident wavelength at 780 nm vs rotating azimuthal angle of the linear polarization of the exciting laser beam. Insets show near-field intensity $|E|^2$ distributions at the polarization directions of $\theta = 0°$ and $\theta = 45°$. Scale bar of the SEM image is 100 nm.

the polarization angle does not affect the SHG signal in this case, as the structural symmetry in the $x-y$ plane in always constant. However, as can be seen in the insets of Figure 2b, the near-field distributions defined as $|E|^2$ vary together with the polarization direction. In other words, both linear (see Figure 1b) and nonlinear (see Figure 2b) responses of plasmonic monomers are symmetric.

However, we next demonstrate that symmetric plasmonic oligomers *do not* follow this principle. Figure 3 displays experimentally measured SHG from pentamers I and II, when pumped at two different wavelengths and rotating the polarization angle of the pump. The two wavelengths are chosen as the representative features in the spectrum: the Fano resonance[34,49] occurring at 780 nm and the maximum near-field gap localization[24] occurring at 820 nm. The measured SHG signals shown in Figure 3c and d both reveal significant fluctuations of the SHG signal when rotating the polarization angle of the pump from $\theta = 0°$ to $\theta = 90°$. Over a full rotation cycle of the pump polarization angle, the SHG signal oscillates from a minimum at $\theta = 45°$ to maximum at $\theta = 0°$ and $\theta = 90°$, directly corresponding to the alignment of polarization with the discrete symmetry of the pentamers. Figure 3a and b demonstrate the simulated near-field intensity at both the wavelengths in pentamers I and II and also a correlation between near-field localization and fluctuations in the SHG signal. It is therefore apparent that, by rotating the pump polarization, the near-field distribution profile changes and affects the SHG, enabling the nonlinear far-field spectroscopy to detect the profile variation. This measurement is thereby able to reveal the underlying symmetry of the pentamer, which is otherwise *not observable* from the variation of the polarization angle in linear far- spectroscopy (see Figure 1b), due to symmetry considerations.[28] We notice that this modulation of the SHG signal is *not* directly proportional to $\cos^4\theta + \sin^4\theta$, and it can be attributed to a local overlap of the electric near field from x- and y-polarized plane waves, thereby contributing to SHG and creating interference of the SH fields (see Supporting Information).

As an extension, we can detect that the sharp triangular edges of pentamer II have not led to a significant change in the maximum amount of SHG in Figure 3c compared to the circular edges of pentamer I in Figure 3d; however they have led to a difference in the contrast between the maximum and minimum values of the SH signal, approximately by a factor of 2. Meanwhile, these results show the importance of both near-field enhancements in the gaps, the so-called hot-spots, and near-field distributions. Previously, it has been suggested that more localized and larger field enhancements in the gaps can increase the nonlinear signal at the nanoscale.[18,38,50−52] But as revealed here, near-field distribution can also play an important role to enhance the signal. It is found that for all cases, for fixed wavelengths, the maximum SHG intensity occurs at $\theta = 0°$ incident polarization, which presents more localized and enhanced fields than those for the $\theta = 45°$ polarization case. In contrast, for a fixed polarization angle, our SHG measurements performed at different wavelengths show a larger signal at 780 nm, where one can see less intense and more distributed near fields. It is likely that 780 nm has a better overlap with the SH resonances, compared to the 820 nm resonance. Therefore, this suggests it is necessary to consider combined effects of both near-field intensity and distribution for SHG in plasmonic structures, rather than solely the influence of near-field localization.

This technique allows us to detect changes in the near-field distribution around an isotropic nanostructure that cannot be detected from the linear transmission, while also bypassing a number of limitations of existing near-field measurement techniques when the given nanostructure becomes very small. Translation of far-field linear spectra[9] cannot be used in this respect, because symmetric structures exhibit far-field-invariant spectra. Indeed, a number of current near-field scanning techniques also have limitations for very small nanostructures. Near-field scanning optical microscopy (NSOM) is the most common technique for fairly large nanostructures, but this technique is limited to resolutions around 80−90 nm for aperture tip NSOM[53] or around 20 nm for apertureless NSOM,[28] while such probes are also quite large and lead to significant perturbation of the near field of investigated objects. Two-photon luminescence of a gold tip has also been suggested to image hot-spots of gold nanoparticles upon illumination;[54] however the interference between the wave scattered from a

DOI: 10.1021/acsphotonics.6b00902
ACS Photonics 2017, 4, 454−461

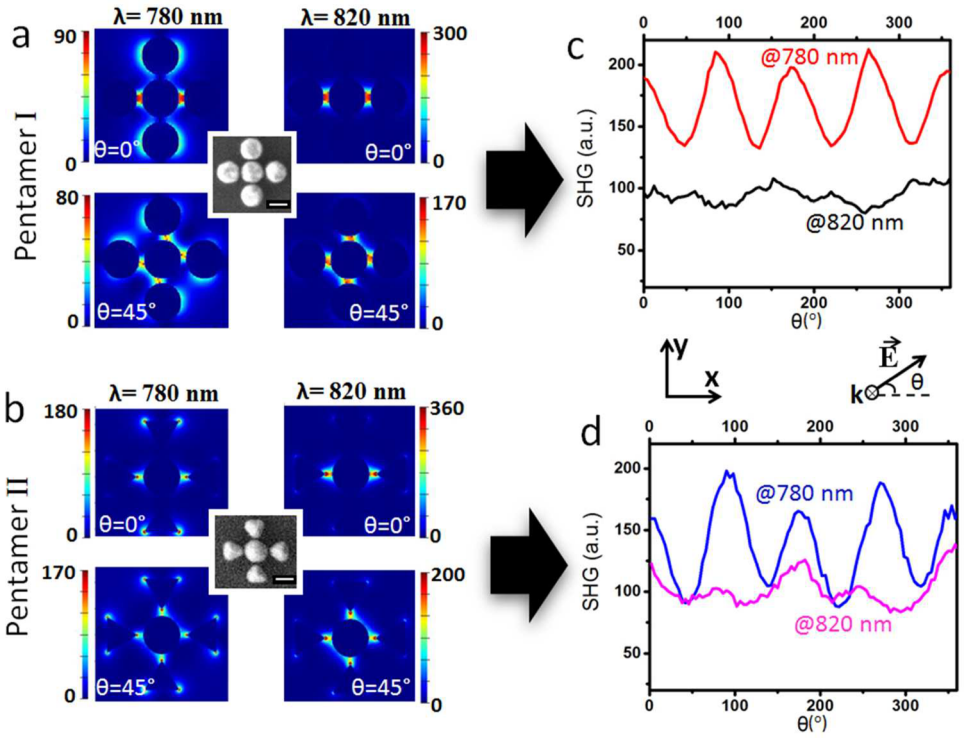

Figure 3. Nonlinear SHG symmetry breaking. Simulated near-field intensity, $|E|^2$, distribution of (a) pentamer I and (b) pentamer II, at 780 and 820 nm, and normalized by the electric field intensity of the applied plane wave. (c and d) Measured SHG spectrum of the corresponding pentamers at 780 and 820 nm vs rotating azimuthal angle of the linear polarization of the exciting laser beam. Scale bar of SEM images is 100 nm.

probe and the waves scattered from a confocally illuminated nanostructure obscures the signal. Therefore, the method presented in this paper can be employed as a versatile tool to identify subtle changes in the near-field distribution without facing aforementioned disadvantages. Recently, a similar approach has been recently employed to unveil the anapole near-field intensity distributions in a single germanium nanodisk,[55] where third-harmonic generation processes through resonant modes in dielectric nanostructures were exploited for the development of high-efficiency photon upconversion nanosystems.

In order to get deeper physical insight, we develop a theoretical model to investigate this nonlinear variation. While the surface quadratic susceptibility is given by a tensor $\overline{\overline{\chi}}^{(2)}$, we restrict our consideration to the most dominant term $\chi^{(2)}_{\perp\perp\perp}$ that describes the scalar quadratic susceptibility for electric fields oriented normal to the surface.[36] Unlike the cross terms of the surface quadratic susceptibility ($\chi^{(2)}_{\perp\parallel\perp}$ and $\chi^{(2)}_{\perp\perp\parallel}$), the capacity of $\chi^{(2)}_{\perp\perp\perp}$ to alter the symmetry of linear fields is unclear, because it preserves the original electric field orientation. Here we explore the *nonlinear* symmetry breaking of optical fields from $\chi^{(2)}_{\perp\perp\perp}$ processes, for which it is convenient to work in terms of symmetry groups and their irreducible representations.[56] The scattering geometries under consideration are invariant under all operations of the C_n cyclic symmetry group, being discrete rotations of $2\pi/n$ about a principal axis, where we assume $n \geq 3$ implicitly herein. An external plane wave can be described by its spatial distribution of the electric field $E^{(0)}$, which we can then separate according to different transformation properties under the symmetry operations of C_n. Specifically, $E^{(0)}$ can be written as a linear combination of some partial contributions $E^{(0)}_\Gamma$, which are the electric field distributions that each transform under symmetry operations according to a different irreducible representation Γ.

$$E^{(0)}(x) = \sum_\Gamma a_\Gamma E^{(0)}_\Gamma(x)$$

Here x is a position vector and a_Γ are complex coefficients. This decomposition can be performed on any external field, and the Supporting Information shows that the linear (first-order) internal fields $E^{(1)}_\Gamma$ induced by each $E^{(0)}_\Gamma$ and also the surface normal component of $E^{(1)}_\Gamma$ relevant for $\chi^{(2)}_{\perp\perp\perp}$ transform under symmetry operations according to Γ. In essence, the symmetry of the fields is never broken by the anisotropy and local surface constraints of $\chi^{(2)}_{\perp\perp\perp}$. This is of significance when excitation comes from plane waves propagating parallel to the principal rotation axis in C_n, which requires only a single irreducible representation $\Gamma = E_1$ (e.g., see Table 1 for C_4). More specifically, any externally applied fields that transform according to the $\Gamma = E_1$ irreducible representation of the C_n symmetry group can be arbitrarily rotated about the principal axis without affecting the total scattered power. This has

Table 1. Character Table for the C_4 Symmetry Group: Rows Are Irreducible Representations (A_1, B_1, E_1); Columns Are Symmetry Operations (identity: $\hat{E}$, rotations: $\hat{C}_2$, $\hat{C}_4$, $(\hat{C}_4)^3$), and Indices Denote Effect of Each Symmetry Operation

	$\hat{E}$	$\hat{C}_2$	$\hat{C}_4$	$(\hat{C}_4)^3$	examples for vector $[x; y; z]$ (z = principal axis)
A_1	1	1	1	1	$x^2 + y^2, z^2, z$
B_1	1	1	−1	−1	$x^2 - y^2, xy$
E_1	$\begin{Bmatrix}1\\1\end{Bmatrix}$	$\begin{Bmatrix}-1\\-1\end{Bmatrix}$	$\begin{Bmatrix}i\\-i\end{Bmatrix}$	$\begin{Bmatrix}-i\\i\end{Bmatrix}$	$\begin{Bmatrix}x + iy\\x - iy\end{Bmatrix}$

DOI: 10.1021/acsphotonics.6b00902
ACS Photonics 2017, 4, 454−461

previously been explained for the polarization independence of the linear scattering, absorption, and extinction cross sections due to C_n symmetry.[28] In our C_4 pentamers, the induced quadratic nonlinear polarization must therefore transform differently to E_1; otherwise symmetry would ensure the total radiated power at the SH frequency does not depend on the polarization angle of the normally incident plane wave. Further details are provided in the Supporting Information.

However, given the surface normal component of $E_\Gamma^{(1)}$ transforms as Γ, we know the quadratic nonlinear polarization from $\chi_{\perp\perp\perp}^{(2)}$ transforms as $(\Gamma)^2$. This describes *different* transformation behavior from Γ, provided Γ does not contain solely identity operations. To explicitly consider SHG from a normally incident plane wave illuminating an object with C_4 symmetry, we refer to Table 1. The total fields produced under the plane wave excitation transform as E_1, but the transformation properties of the SH fields, being described by $(E_1)^2$, are equivalent to transformation properties described by the A_1 and B_1 irreducible representations, which encompass polarization-dependent optical responses. The equivalence of $(E_1)^2$ to A_1 and B_1 can be seen by taking different products of the rows of E_1 in Table 1. This shows that *the symmetry of the nonlinear fields is changed* or becomes *broken* compared to the symmetry of the source linear fields, and this is purely a result of the quadratic nonlinear process. Because SHG does not transform according to E_1, the geometric symmetry now permits dependence on the polarization of a normal incidence plane wave pump at fundamental frequency, in full agreement with our experimental studies.

In Figures 4a–c, we present numerical simulations for the scattering of a gold pentamer I with experimental dimensions (disk diameters 140 nm and gaps 20 nm), on a glass substrate and illuminated by a normally incident plane wave. We calculate the linear (the first-order) internal fields $E^{(1)}$ and plot the total scattered power at both 780 and 820 nm as a function of the polarization angle for the total linear scattering (Figure 4a) and the linear scattering produced by the surface-normal component of $E^{(1)}$ in a 10 nm (volumetric) surface layer around each nanoparticle (Figure 4b). The 780 and 820 nm spectra are normalized to the corresponding average scattered power at 820 nm. Both sets of linear scattering data are completely independent of the polarization angle of the incident plane wave, as expected because these fields maintain E_1 symmetry of the incident plane wave. However, in Figure 4c, we plot additionally the normalized total nonlinear scattering, using the square of the surface-normal component of $E^{(1)}$ in the 10 nm surface layer of Figure 4b as an externally applied field. This represents SH radiation at 390 and 410 nm, respectively, and it clearly oscillates with the polarization angle, in full agreement with the above discussion on breaking E_1 symmetry. These data match qualitatively the measurements shown in Figure 3, with 820 nm modulation being smaller than that at 780 nm. However, a contrast between 780 and 820 nm modulations in the experiment is greater, being attributed to the extinction minimum of the Fano resonance of the pentamer I being blue-shifted in numerical simulations; see Figure 1. Calculations are performed using COMSOL, and gold permittivity data taken from Johnson and Christy.[57] Further information is provided in the Methods.

These findings pave the way toward experimental studies of the symmetry classes for nanostructures and even a wide range of molecules in nature. Indeed, light–matter interactions are already used to study molecular systems, including numerical

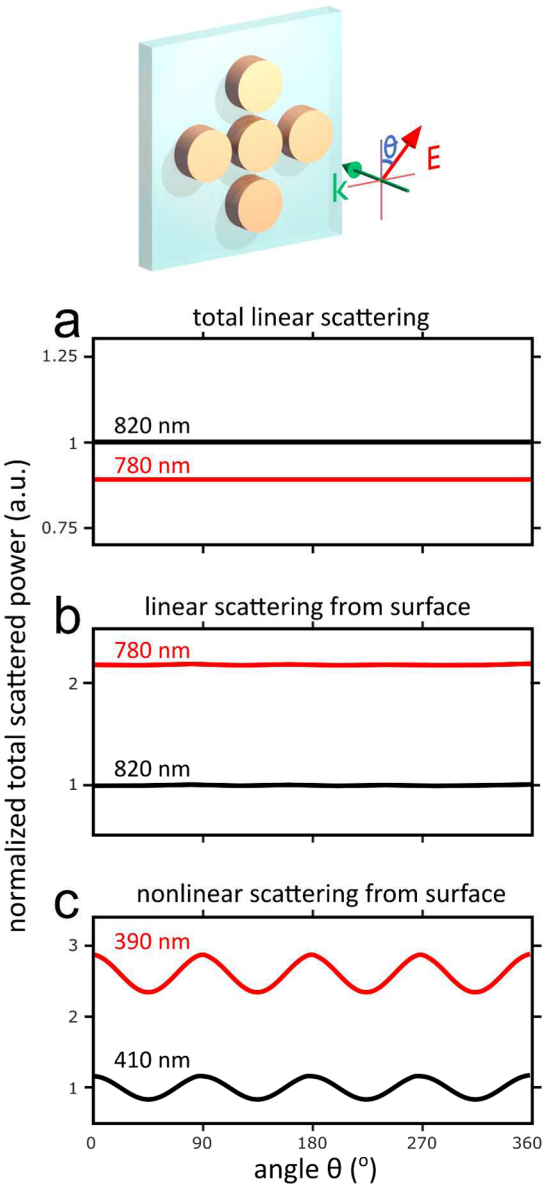

Figure 4. Total scattered power from a gold nanodisk pentamer, on a glass substrate, under a normally incident plane wave with 780 and 820 nm wavelengths, as a function of its polarization angle. Diameter of disks and gaps are 140 and 20 nm, respectively. (a) Total linear scattering, (b) linear scattering from the surface-normal components of the internal fields, and (c) SH scattering from the square of the surface-normal components of the internal fields.

predictions of the interaction between an intense laser field and an electron moving in molecules and atoms,[39,58] and experimental measurements, such as ultrafast charge dynamics in amino acids[59] or migration of electron–hole pairs immediately after ionization of molecules.[60] We believe that our findings can be applied to molecular physics, where the molecular symmetry can lead to the appearance and complete disappearance of certain peaks in the SHG spectra. This is similar to a recent approach for revealing symmetries of molecules by SH spectroscopy when illuminating molecular structures through circular polarizations.[41] The symmetry breaking is associated with the transformation from linear to SH fields, and it should therefore apply equally to molecules as it does to nanostructures.

DOI: 10.1021/acsphotonics.6b00902
ACS Photonics 2017, 4, 454–461

In conclusion, we have reported a significant asymmetric variation of nonlinear optical response from symmetric plasmonic oligomers. By monitoring the SHG signal against the polarization rotation of the incident light, we have detected that the nonlinear response of symmetric oligomers varies with the polarization angle, while their linear response remains independent of the polarization angle. Our approach can be employed for detecting the symmetry classes of oligomers, and it can be extended to detect the symmetry classes of many molecules in nature. Also, our finding can assist in characterizing changes in the near-field patterns in symmetric nanostructures beyond the limitations of the current near-field microscopy techniques.

METHODS

The Au pentamers consist of a single central circular disk surrounded by either four circular disks (pentamer I) or four triangular-shaped nanoparticles (pentamer II) on a quartz substrate. Arrays of these pentamers are fabricated by an electron beam lithography system (Elonix 100 kV EBL). Each array has dimensions of 50 × 50 μm^2. A 2 nm thick Ti film was deposited on the quartz substrate by e-beam evaporation (EB03 BOC Edwards) to improve the adhesion between Au and quartz, followed by the evaporation of a 60 nm thick Au film and spin-coating a 50 nm thick layer of hydrogen silsesquioxane as a negative electroresist. After baking the sample at 200 °C for 2 min, a combined process of e-beam exposure, development, and ion-milling was performed to create well-defined Au nanoparticles on the substrate. The surface morphology of the fabricated structures was characterized by high-resolution scanning electron microscopy (SEM) and atomic force microscopy (AFM). Extinction (1 − transmission) was measured with a home-built white-light spectrometer that uses a tungsten light bulb as a broadband optical source and an optical spectrum analyzer detection. For the SHG measurements, we used an optical setup based on a Coherent Micra Ti:sapphire laser tuned in the spectral region of 780−820 nm. The pulse width of the pump laser was about 40 fs, and the repetition rate was 80 MHz. The light was directed to the Hamamatsu H10682-210 photon counter module through a set of Schott BG39 and BG3 filters in order to remove the unwanted pump radiation. Maximum mean power of the pump beam in the sample plane was up to 5 mW. Nonlinear signals were normalized over the surface area of the structures (see the setup schematic in the Supporting Information).

Three-dimensional Lumerical FDTD simulations were employed to calculate the extinction cross sections of individual nanostructures. Simulations of second-harmonic generation were performed with the frequency domain solver in Comsol for a type I pentamer on a glass (n = 1.45) substrate. The square of the surface normal components of the total electric field induced by a plane wave provided the external current density distributions to model the source of second-harmonic fields. Nonlinear signal was defined as the integral of the total outgoing time-averaged power flow at the second-harmonic wavelength.

ASSOCIATED CONTENT

Supporting Information

The Supporting Information is available free of charge on the ACS Publications website at DOI: 10.1021/acsphotonics.6b00902.

Derivations to show that polarization-dependence of the second-harmonic generation implies the quadratic nonlinearity has necessarily broken the symmetry of the linear response; schematic of the nonlinear measurement setup (PDF)

AUTHOR INFORMATION

Corresponding Author

*E-mail: mohsen.rahmani@anu.edu.au.

ORCID

Mohsen Rahmani: 0000-0001-9268-4793
Ben Hopkins: 0000-0002-4570-4269
Andrey E. Miroshnichenko: 0000-0001-9607-6621
Dragomir N. Neshev: 0000-0002-4508-8646

Notes

The authors declare no competing financial interest.

ACKNOWLEDGMENTS

The authors acknowledge the funding support provided by the Australian Research Council (ARC). M.R sincerely appreciates funding from an ARC Discover Early Career Research Fellowship ((DE170100250). B.H. acknowledges support from the Erasmus Mundus NANOPHI project, contract number 2013 5659/002-001, and much COMSOL-based guidance from L. Carletti and C. De Angelis. R.C. acknowledges a grant from Consejo Nacional de Ciencia y Tecnología (CONACYT), México. The authors appreciate the use of facilities of the Data Storage Institute, Agency for Science, Technology and Research (A*STAR), Singapore, for the sample fabrication and imaging, as well as Australian National Fabrication Facility (ANFF)−the ACT Node, and the Russian Foundation for Basic Research (15-32-21156), for characterizations. M.R., A.E.M., and R.C. appreciate a funding from Australia-Germany Joint Research Cooperation Scheme.

REFERENCES

(1) Miroshnichenko, A. E.; Flach, S.; Kivshar, Y. S. Fano resonances in nanoscale structures. *Rev. Mod. Phys.* **2010**, *82*, 2257−2298.

(2) Luk'yanchuk, B.; Zheludev, N. I.; Maier, S. A.; Halas, N. J.; Nordlander, P.; Giessen, H.; Chong, C. T. The Fano resonance in plasmonic nanostructures and metamaterials. *Nat. Mater.* **2010**, *9*, 707−715.

(3) Halas, N. J.; Lal, S.; Chang, W.-S.; Link, S.; Nordlander, P. Plasmons in strongly coupled metallic nanostructures. *Chem. Rev.* **2011**, *111*, 3913−3961.

(4) Rahmani, M.; Luk'yanchuk, B.; Hong, M. Fano resonance in novel plasmonic nanostructures. *Laser Photon. Rev.* **2013**, *7*, 329−349.

(5) Bozhevolnyi, S. *Plasmonic Nanoguides and Circuits*; Pan Stanford: Singapore, 2009.

(6) Durach, M.; Rusina, A.; Stockman, M. I.; Nelson, K. Toward full spatiotemporal control on the nanoscale. *Nano Lett.* **2007**, *7*, 3145−3149.

(7) Hao, F.; Sonnefraud, Y.; Dorpe, P. V.; Maier, S. A.; Halas, N. J.; Nordlander, P. Symmetry breaking in plasmonic nanocavities: subradiant LSPR sensing and a tunable Fano resonance. *Nano Lett.* **2008**, *8*, 3983−3988.

(8) Rahmani, M.; Lukiyanchuk, B.; Nguyen, T.; Tahmasebi, T.; Lin, Y.; Liew, T.; Hong, M. Influence of symmetry breaking in pentamers on Fano resonance and near-field energy localization. *Opt. Mater. Express* **2011**, *1*, 1409−1415.

(9) Liu, N.; Hentschel, M.; Weiss, T.; Alivisatos, A. P.; Giessen, H. Three-dimensional plasmon rulers. *Science* **2011**, *332*, 1407−1410.

(10) Camacho-Morales, R.; Rahmani, M.; Kruk, S.; Wang, L.; Xu, L.; Smirnova, D. A.; Solntsev, A. S.; Miroshnichenko, A.; Tan, H. H.;

DOI: 10.1021/acsphotonics.6b00902
ACS Photonics 2017, 4, 454−461

Karouta, F.; Naureen, S.; Vora, K.; Carletti, L.; De Angelis, C.; Jagadish, C.; Kivshar, Y.; Neshev, D. N. Nonlinear generation of vector beams from AlGaAs nanoantennas. *Nano Lett.* **2016**, *16*, 7191−7197.
(11) Hao, F.; Nordlander, P.; Sonnefraud, Y.; Dorpe, P. V.; Maier, S. A. Tunability of subradiant dipolar and Fano-type plasmon resonances in metallic ring/disk cavities: implications for nanoscale optical sensing. *ACS Nano* **2009**, *3*, 643−652.
(12) Verellen, N.; Sonnefraud, Y.; Sobhani, H.; Hao, F.; Moshchalkov, V. V.; Dorpe, P. V.; Nordlander, P.; Maier, S. A. Fano resonances in individual coherent plasmonic nanocavities. *Nano Lett.* **2009**, *9*, 1663−1667.
(13) Wu, C.; Khanikaev, A. B.; Adato, R.; Arju, N.; Yanik, A. A.; Altug, H.; Shvets, G. Fano-resonant asymmetric metamaterials for ultrasensitive spectroscopy and identification of molecular monolayers. *Nat. Mater.* **2012**, *11*, 69−75.
(14) Davoyan, A. R.; Shadrivov, I. V.; Kivshar, Y. S. Nonlinear plasmonic slot waveguides. *Opt. Express* **2008**, *16*, 21209−21214.
(15) Salgueiro, J. R.; Kivshar, Y. S. Nonlinear plasmonic directional couplers. *Appl. Phys. Lett.* **2010**, *97*, 081106.
(16) Davoyan, A. R.; Shadrivov, I. V.; Kivshar, Y. S. Self-focusing and spatial plasmon-polariton solitons. *Opt. Express* **2009**, *17*, 21732−21737.
(17) Marini, A.; Skryabin, D. Ginzburg-Landau equation bound to the metal-dielectric interface and transverse nonlinear optics with amplified plasmon polaritons. *Phys. Rev. A: At., Mol., Opt. Phys.* **2010**, *81*, 033850.
(18) Linnenbank, H.; Grynko, Y.; Förstner, J.; Linden, S. Second harmonic generation spectroscopy on hybrid plasmonic/dielectric nanoantennas. *Light: Sci. Appl.* **2016**, *5*, e16013.
(19) Kravtsov, V.; Ulbricht, R.; Atkin, J. M.; Raschke, M. B. Plasmonic nanofocused four-wave mixing for femtosecond near-field imaging. *Nat. Nanotechnol.* **2016**, *11*, 459−464.
(20) Bao, K.; Mirin, N. A.; Nordlander, P. Fano resonances in planar silver nanosphere clusters. *Appl. Phys. A: Mater. Sci. Process.* **2010**, *100*, 333−339.
(21) Hentschel, M.; Saliba, M.; Vogelgesang, R.; Giessen, H.; Alivisatos, A. P.; Liu, N. Transition from isolated to collective modes in plasmonic oligomers. *Nano Lett.* **2010**, *10*, 2721−2726.
(22) Lassiter, J. B.; Sobhani, H.; Fan, J. A.; Kundu, J.; Capasso, F.; Nordlander, P.; Halas, N. J. Fano resonances in plasmonic nanoclusters: geometrical and chemical tunability. *Nano Lett.* **2010**, *10*, 3184−3189.
(23) Rahmani, M.; Lei, D. Y.; Giannini, V.; Lukiyanchuk, B.; Ranjbar, M.; Liew, T. Y. F.; Hong, M.; Maier, S. A. Subgroup decomposition of plasmonic resonances in hybrid oligomers: modeling the resonance lineshape. *Nano Lett.* **2012**, *12*, 2101−2106.
(24) Rahmani, M.; Lukiyanchuk, B.; Tahmasebi, T.; Lin, Y.; Liew, T.; Hong, M. Polarization-controlled spatial localization of near-field energy in planar symmetric coupled oligomers. *Appl. Phys. A: Mater. Sci. Process.* **2012**, *107*, 23−30.
(25) Miroshnichenko, A. E.; Kivshar, Y. S. Fano resonances in all-dielectric oligomers. *Nano Lett.* **2012**, *12*, 6459−6463.
(26) Chong, K. E.; Hopkins, B.; Staude, I.; Miroshnichenko, A. E.; Dominguez, J.; Decker, M.; Neshev, D. N.; Brener, I.; Kivshar, Y. S. Observation of Fano resonances in all-dielectric nanoparticle oligomers. *Small* **2014**, *10*, 1985−1990.
(27) Yorulmaz, M.; Hoggard, A.; Zhao, H.; Wen, F.; Chang, W.-S.; Halas, N. J.; Nordlander, P.; Link, S. Absorption Spectroscopy of an Individual Fano Cluster. *Nano Lett.* **2016**, *16*, 6497−6503.
(28) Rahmani, M.; Yoxall, E.; Hopkins, B.; Sonnefraud, Y.; Kivshar, Y.; Hong, M.; Phillips, C.; Maier, S. A.; Miroshnichenko, A. E. Plasmonic nanoclusters with rotational symmetry: polarization-invariant far-field response vs changing near-field distribution. *ACS Nano* **2013**, *7*, 11138−11146.
(29) Rahmani, M.; Tahmasebi, T.; Lin, Y.; Lukiyanchuk, B.; Liew, T.; Hong, M. Influence of plasmon destructive interferences on optical properties of gold planar quadrumers. *Nanotechnology* **2011**, *22*, 245204.
(30) Liu, N.; Mukherjee, S.; Bao, K.; Brown, L. V.; Dorfmüller, J.; Nordlander, P.; Halas, N. J. Magnetic plasmon formation and propagation in artificial aromatic molecules. *Nano Lett.* **2011**, *12*, 364−369.
(31) Thyagarajan, K.; Rivier, S.; Martin, O. J. In *Nonlinear Plasmonics of Metallic Heptamers*; SPIE OPTO; International Society for Optics and Photonics, 2012; pp 82691Z-82691Z−6.
(32) Zhang, Y.; Wen, F.; Zhen, Y.-R.; Nordlander, P.; Halas, N. J. Coherent Fano resonances in a plasmonic nanocluster enhance optical four-wave mixing. *Proc. Natl. Acad. Sci. U. S. A.* **2013**, *110*, 9215−9219.
(33) Thyagarajan, K.; Butet, J. r. m.; Martin, O. J. Augmenting second harmonic generation using Fano resonances in plasmonic systems. *Nano Lett.* **2013**, *13*, 1847−1851.
(34) Butet, J.; Martin, O. J. Fano resonances in the nonlinear optical response of coupled plasmonic nanostructures. *Opt. Express* **2014**, *22*, 29693−29707.
(35) Shcherbakov, M. R.; Shorokhov, A. S.; Neshev, D. N.; Hopkins, B.; Staude, I.; Melik-Gaykazyan, E. V.; Ezhov, A. A.; Miroshnichenko, A. E.; Brener, I.; Fedyanin, A. A. Nonlinear interference and tailorable third-harmonic generation from dielectric oligomers. *ACS Photonics* **2015**, *2*, 578−582.
(36) Butet, J.; Brevet, P.-F.; Martin, O. J. Optical second harmonic generation in plasmonic nanostructures: From fundamental principles to advanced applications. *ACS Nano* **2015**, *9*, 10545−10562.
(37) Metzger, B.; Hentschel, M.; Giessen, H. Ultrafast Nonlinear Plasmonic Spectroscopy: From Dipole Nanoantennas to Complex Hybrid Plasmonic Structures. *ACS Photonics* **2016**, *3*, 1336−1350.
(38) Liu, S.-D.; Leong, E. S. P.; Li, G.-C.; Hou, Y.; Deng, J.; Teng, J. H.; Ong, H. C.; Lei, D. Y. Polarization-Independent Multiple Fano Resonances in Plasmonic Nonamers for Multimode-Matching Enhanced Multiband Second-Harmonic Generation. *ACS Nano* **2016**, *10*, 1442−1453.
(39) Reich, D. M.; Madsen, L. B. Illuminating Molecular Symmetries with Bicircular High-Order-Harmonic Generation. *Phys. Rev. Lett.* **2016**, *117*, 133902.
(40) Reich, D. M.; Madsen, L. B. Rotating-frame perspective on high-order-harmonic generation of circularly polarized light. *Phys. Rev. A: At., Mol., Opt. Phys.* **2016**, *93*, 043411.
(41) Baykusheva, D.; Ahsan, M. S.; Lin, N.; Wörner, H. J. Bicircular High-Harmonic Spectroscopy Reveals Dynamical Symmetries of Atoms and Molecules. *Phys. Rev. Lett.* **2016**, *116*, 123001.
(42) Alonso-Gonzalez, P.; Schnell, M.; Sarriugarte, P.; Sobhani, H.; Wu, C.; Arju, N.; Khanikaev, A.; Golmar, F.; Albella, P.; Arzubiaga, L. Real-space mapping of Fano interference in plasmonic metamolecules. *Nano Lett.* **2011**, *11*, 3922−3926.
(43) Bachelier, G.; Butet, J.; Russier-Antoine, I.; Jonin, C.; Benichou, E.; Brevet, P.-F. Origin of optical second-harmonic generation in spherical gold nanoparticles: Local surface and nonlocal bulk contributions. *Phys. Rev. B: Condens. Matter Mater. Phys.* **2010**, *82*, 235403.
(44) Butet, J.; Gallinet, B.; Thyagarajan, K.; Martin, O. J. Second-harmonic generation from periodic arrays of arbitrary shape plasmonic nanostructures: a surface integral approach. *J. Opt. Soc. Am. B* **2013**, *30*, 2970−2979.
(45) Aouani, H.; Rahmani, M.; Navarro-Cía, M.; Maier, S. A. Third-harmonic-upconversion enhancement from a single semiconductor nanoparticle coupled to a plasmonic antenna. *Nat. Nanotechnol.* **2014**, *9*, 290−294.
(46) Kauranen, M.; Zayats, A. V. Nonlinear plasmonics. *Nat. Photonics* **2012**, *6*, 737−748.
(47) Zhang, Y.; Grady, N. K.; Ayala-Orozco, C.; Halas, N. J. Three-dimensional nanostructures as highly efficient generators of second harmonic light. *Nano Lett.* **2011**, *11*, 5519−5523.
(48) Chen, S.; Li, G.; Zeuner, F.; Wong, W. H.; Pun, E. Y. B.; Zentgraf, T.; Cheah, K. W.; Zhang, S. Symmetry-selective third-harmonic generation from plasmonic metacrystals. *Phys. Rev. Lett.* **2014**, *113*, 033901.
(49) Shorokhov, A. S.; Melik-Gaykazyan, E. V.; Smirnova, D. A.; Hopkins, B.; Chong, K. E.; Choi, D.-Y.; Shcherbakov, M. R.;

DOI: 10.1021/acsphotonics.6b00902
ACS Photonics 2017, 4, 454−461

Miroshnichenko, A. E.; Neshev, D. N.; Fedyanin, A. A.; Kivshar, Y. S. Multifold Enhancement of Third-Harmonic Generation in Dielectric Nanoparticles Driven by Magnetic Fano Resonances. *Nano Lett.* **2016**, *16*, 4857−4861.
(50) Aouani, H.; Navarro-Cia, M.; Rahmani, M.; Sidiropoulos, T. P.; Hong, M.; Oulton, R. F.; Maier, S. A. Multiresonant broadband optical antennas as efficient tunable nanosources of second harmonic light. *Nano Lett.* **2012**, *12*, 4997−5002.
(51) Celebrano, M.; Wu, X.; Baselli, M.; Großmann, S.; Biagioni, P.; Locatelli, A.; De Angelis, C.; Cerullo, G.; Osellame, R.; Hecht, B. Mode matching in multiresonant plasmonic nanoantennas for enhanced second harmonic generation. *Nat. Nanotechnol.* **2015**, *10*, 412−417.
(52) Gennaro, S. D.; Rahmani, M.; Giannini, V.; Aouani, H.; Sidiropoulos, T. P.; Navarro-Cía, M.; Maier, S. A.; Oulton, R. F. The Interplay of Symmetry and Scattering Phase in Second Harmonic Generation from Gold Nanoantennas. *Nano Lett.* **2016**, *16*, 5278−5285.
(53) Bao, W.; Borys, N. J.; Ko, C.; Suh, J.; Fan, W.; Thron, A.; Zhang, Y.; Buyanin, A.; Zhang, J.; Cabrini, S. Visualizing nanoscale excitonic relaxation properties of disordered edges and grain boundaries in monolayer molybdenum disulfide. *Nat. Commun.* **2015**, 6.799310.1038/ncomms8993
(54) Jäger, S.; Kern, A. M.; Hentschel, M.; Jäger, R.; Braun, K.; Zhang, D.; Giessen, H.; Meixner, A. J. Au nanotip as luminescent near-field probe. *Nano Lett.* **2013**, *13*, 3566−3570.
(55) Grinblat, G.; Li, Y.; Nielsen, M. P.; Oulton, R. F.; Maier, S. A. Efficient Third Harmonic Generation and Nonlinear Sub-Wavelength Imaging at a Higher-Order Anapole Mode in a Single Germanium Nanodisk. *ACS Nano* **2016**, *11*, 953.
(56) Dresselhaus, M. S.; Dresselhaus, G.; Jorio, A. *Group Theory: Application to the Physics of Condensed Matter*; Springer Science & Business Media, 2007.
(57) Johnson, P. B.; Christy, R.-W. Optical constants of the noble metals. *Phys. Rev. B* **1972**, *6*, 4370.
(58) Ceccherini, F.; Bauer, D.; Cornolti, F. Dynamical symmetries and harmonic generation. *J. Phys. B: At., Mol. Opt. Phys.* **2001**, *34*, 5017.
(59) Calegari, F.; Ayuso, D.; Trabattoni, A.; Belshaw, L.; De Camillis, S.; Anumula, S.; Frassetto, F.; Poletto, L.; Palacios, A.; Decleva, P. Ultrafast electron dynamics in phenylalanine initiated by attosecond pulses. *Science* **2014**, *346*, 336−339.
(60) Kraus, P.; Mignolet, B.; Baykusheva, D.; Rupenyan, A.; Horný, L.; Penka, E.; Grassi, G.; Tolstikhin, O. I.; Schneider, J.; Jensen, F. Measurement and laser control of attosecond charge migration in ionized iodoacetylene. *Science* **2015**, *350*, 790−795.

DOI: 10.1021/acsphotonics.6b00902
ACS Photonics 2017, 4, 454−461